Geodetic secular velocity errors due to interannual surface loading deformation,

Alvaro Santamaria-Gomez, Anthony Mémin

Geophysical Journal International

Geophys. J. Int. (2015) **202,** 763–767
GJI Gravity, geodesy and tides

doi: 10.1093/gji/ggv190

EXPRESS LETTER

Geodetic secular velocity errors due to interannual surface loading deformation

Alvaro Santamaría-Gómez[1,2] and Anthony Mémin[3,4]

[1] *LIENSs, Université de La Rochelle/CNRS, La Rochelle, France. E-mail: alvaro.santamaria@univ-lr.fr*
[2] *School of Land and Food, University of Tasmania, Hobart, Australia*
[3] *Université Nice Sophia Antipolis, CNRS, IRD, Observatoire de la Côte d'Azur, Géoazur, UMR7329, Valbonne, France*
[4] *School of Physical Sciences, University of Tasmania, Hobart, Australia*

Accepted 2015 April 29. Received 2015 April 28; in original form 2015 March 5

SUMMARY

Geodetic vertical velocities derived from data as short as 3 yr are often assumed to be representative of linear deformation over past decades to millennia. We use two decades of surface loading deformation predictions due to variations of atmospheric, oceanic and continental water mass to assess the effect on secular velocities estimated from short time-series. The interannual deformation is time-correlated at most locations over the globe, with the level of correlation depending mostly on the chosen continental water model. Using the most conservative loading model and 5-yr-long time-series, we found median vertical velocity errors of 0.5 mm yr^{-1} over the continents (0.3 mm yr^{-1} globally), exceeding 1 mm yr^{-1} in regions around the southern Tropic. Horizontal velocity errors were seven times smaller. Unless an accurate loading model is available, a decade of continuous data is required in these regions to mitigate the impact of the interannual loading deformation on secular velocities.

Key words: Time-series analysis; Persistence, memory, correlations, clustering; Transient deformation; Kinematics of crustal and mantle deformation.

1 INTRODUCTION

Secular surface velocities from different techniques (mostly the Global Positioning System, GPS) are used to investigate a wide range of geophysical applications including sea-level change (e.g. Wöppelmann *et al.* 2014) or rheology of the solid Earth (e.g. Mémin *et al.* 2014). It is commonly assumed that reliable velocities can be estimated with at least 3 yr of observations to avoid errors caused by seasonal signals (Blewitt & Lavallée 2002; Bos *et al.* 2010). Importantly, for many of these geophysical applications, the estimated secular velocities are often extrapolated outside the period of the observations and used to represent linear deformation over decades to millennia (Wöppelmann *et al.* 2013).

Unmodelled non-tidal surface loading deformation in geodetic position time-series either increase the noise or bias derived secular velocities depending on the time-series length. This is particularly relevant to the vertical component, where deformation signals are larger. Numerous studies have shown significant impact of non-tidal atmospheric, oceanic and continental water mass loading deformation on geodetic position time-series, especially on the vertical component (e.g. Dach *et al.* 2011; Fritsche *et al.* 2012; van Dam *et al.* 2012).

With respect to coordinate time-series noise, most of these studies have considered the impact of the loading mass deformation in terms of the variance (or rms) reduction when removing the modelled deformation from the position time-series. Such a metric considers variance reduction in the part of the spectrum dominated by uncorrelated (white) noise, but does not address changes to time-correlated noise. However, it is known that position time-series are sensitive to mass loading deformation at longer (interannual) periods (e.g. Tregoning & Watson 2009; Valty *et al.* 2013).

Less attention has been paid to the impact of non-tidal deformation on secular surface velocities. This has been most widely considered in relation to geodetic observations near centres of ice loading change since the deformation signal is often large and time variable (e.g. Groh *et al.* 2014). The effect of non-tidal atmospheric, oceanic and continental water mass loading variations is less well studied.

In this paper, we quantify the impact of interannual mass loading deformation on secular velocities when estimated from short position time-series. In the presence of non-linear deformation, the position time-series are 'coloured' or time-correlated in the spectral domain. Therefore, we characterize the time-correlation of surface deformation at the interannual band to assess velocity errors globally. We then qualitatively assess spatial patterns of velocity errors from 5-yr-long time-series at the regional level with important implications for geophysical interpretation.

2 MODELLED MASS LOADING DEFORMATION

We used loading deformation predictions between January 1993 and August 2014 due to atmospheric and continental water (including soil moisture and snow) mass variations from the European Centre for Medium-Range Weather Forecasts reanalysis (ERA Interim; Dee *et al.* 2011) and oceanic mass variations from the estimating the circulation and climate ocean model (ECCO; Stammer *et al.* 2002). We used global grids between ±80°N/S latitude with spatial resolution of 0.5° available from the University of Strasbourg loading service (http://loading.u-strasbg.fr, last accessed May 2015). We do not include deformation due to present-day ice mass changes because they are not available for the period considered (e.g. King *et al.* 2012a), while we bear in mind this contribution may dominate in glaciated regions. We do not include non-loading hydrogeological processes triggered by water mass variations either (e.g. Nahmani *et al.* 2012).

The modelled deformation was computed based on the Preliminary Reference Earth Model (Dziewonski & Anderson 1981) assuming a spherically stratified and non-rotating Earth with perfectly elastic and isotropic structural relation (SNREI). Computations were expressed within the centre of figure (CF) of the solid Earth frame. To be consistent with the ocean mass loading deformation, and because we are interested in long-period deformation, the ocean response to atmospheric mass changes was assumed to follow the modified inverted barometer effect (Van Dam & Wahr 1987). The resolution of the land/sea mask was 0.10° for atmospheric loading and 0.25° for oceanic and continental water loading, respectively. See Petrov & Boy (2004) for further details on the computed loading deformation.

The computed deformation of each loading contribution was averaged to monthly values. To reduce the amount of data processed while avoiding introducing errors from spatial averaging, the number of gridded values was decimated by 4, resulting in 14 400 deformation time-series spaced horizontally by 2°. The deformation time-series of each loading contribution were then combined to form the total loading deformation. Since the three modelled deformation were originally available in the same regular grid, no interpolation was needed in the combination, avoiding resolution problems at the land–ocean interface. The seasonal signals (annual and semi-annual), mean value and trends were fitted to the total deformation time-series using least squares. The resulting residual time-series spanned almost 22 yr, thereby allowing us to consider non-linear deformation with periods from 2 months to 2 decades. Unless otherwise stated, we address velocity errors on the vertical component where the loading deformation signal is more significant.

3 VELOCITY ERRORS FROM MASS LOADING DEFORMATION

Interannual loading deformation from mass variations was assessed by fitting a power-law noise process to every residual time-series. Details on the noise analysis are provided in the supporting information. The estimated power-law amplitude and spectral index (see Fig. S1) were transformed into equivalent formal velocity uncertainty (at 2σ) using the general formula from Williams (2003a). Formal uncertainties estimated with this formula agree well with uncertainty estimates from inverting the complete covariance matrix (Santamaría-Gómez *et al.* 2011). The resulting velocity uncertainties at 2σ provide the upper-bound velocity error for any continuous period of the chosen length during the last two decades.

Considering 5-yr-long time-series, Fig. 1 shows the geographical distribution of the upper-bound vertical velocity error on a cell-by-cell basis for any 5-yr period between 1993 and 2014. Areas where the velocity error is zero indicate that power-law noise was not significantly detected. Excluding these areas, the median and 95 per cent values of the velocity errors amongst all the cells are 0.3 and 0.7 mm yr^{-1}, respectively. If one considers continental landmasses only, the median and 95 per cent velocity errors become 0.5 and 1.0 mm yr^{-1}, respectively. Localized continental regions over the Equator and southern Tropic are heavily affected by interannual

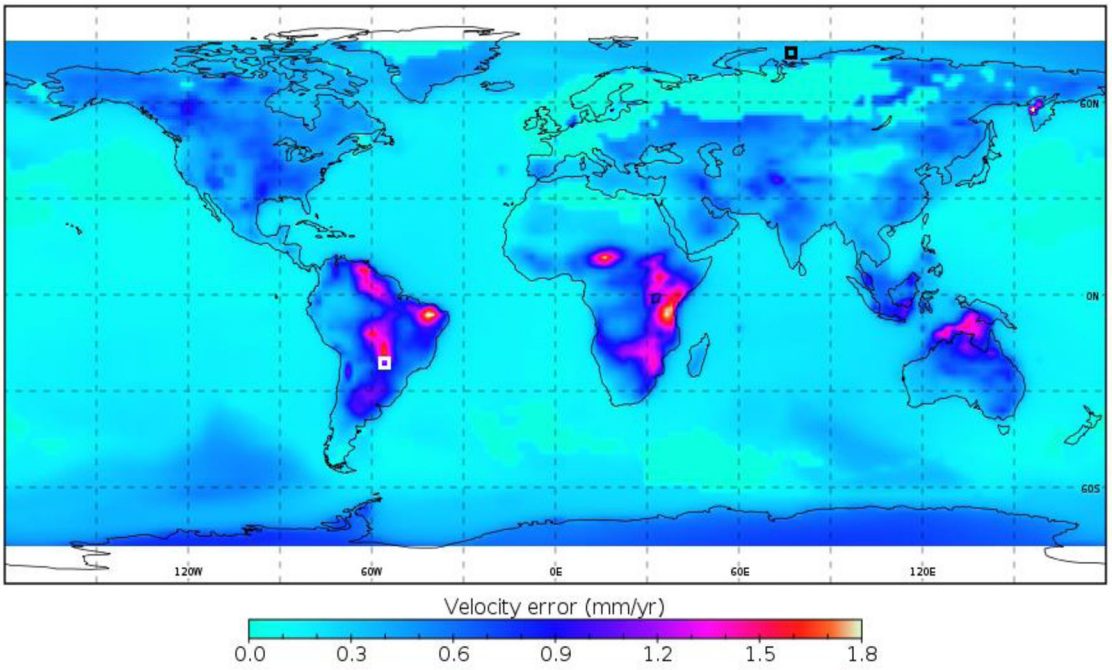

Figure 1. Geographic distribution of the vertical velocity errors (in mm yr^{-1}) for 5 yr of continuous data. Velocity errors are computed from the estimated power-law noise parameters using monthly sampling. Null velocity errors represent areas where power-law noise was not significantly detected over uncorrelated (white) noise. The black and white squares provide the location of the red and blue curves of Fig. 2, respectively.

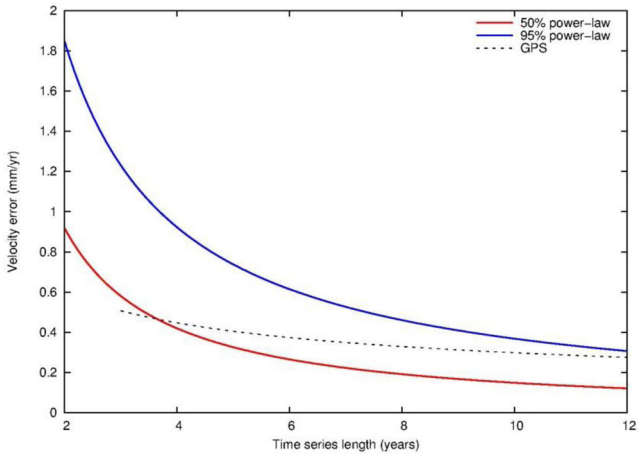

Figure 2. Vertical velocity error (in mm yr^{-1}) as a function of time-series length (in years). The colour lines represent the velocity error at locations where the estimated power-law parameters reach the median (red) and 95 per cent (blue) values among all the cells shown in Fig. 1. The dashed black line represents GPS velocity uncertainties estimated from weekly time-series with a minimum of 3 yr of data.

loading, where velocity errors larger than 1 mm yr^{-1} were found. Considering the horizontal component, velocity errors reduce to 0.04 and 0.1 mm yr^{-1} for the median and 95 per cent values, respectively; around seven times smaller (Fig. S2).

Fig. 2 shows the change of the velocity error with time-series length. Two velocity error curves were estimated at cells exhibiting power-law parameters corresponding to the median and 95 per cent values amongst all the cells. The dotted black line represents the average formal velocity uncertainty in a global GPS velocity field (Santamaría-Gómez *et al.* 2012). This figure shows that, for most of the locations, at least 4 yr of data are needed to avoid velocity errors larger than the GPS velocity uncertainty. At some locations in the Equatorial band more than 10 yr of data are needed.

The spatial pattern in Fig. 1 is qualitatively reproduced in the standard deviation of velocities estimated from overlapping 5-yr windows in the deformation time-series (see Fig. S3). The velocity biases in Fig. S3 are slightly smaller because of the correlation of the velocity estimates from the overlapped data. Excluding areas where power law was not significantly detected, both spatial patterns agree reasonably well with differences smaller than 0.2 mm yr^{-1} (at 95 per cent). This indicates that the power-law process is a good proxy for the long-term non-linear deformation considered here. In addition, using a power-law process to characterize the interannual deformation allows one to estimate the velocity error for any time-series length considered straightforwardly (see Fig. 2). However, neither the power-law process nor the scatter of the trends predict the sign of the velocity error for a specific period.

Without loss of generality, we considered the velocity biases for the periods 2004–2009 and 2009–2014 from the deformation time-series (Fig. 3). During the latter period many GPS stations have been installed around the world within the context of establishment of new regional/national networks. Examples of this are the plate boundary observatory network in western North America for plate deformation, the Antarctic POLENET/ANET network for determination of crustal deformation associated with glacial isostatic adjustment, or the Indonesian Tsunami Early Warning System for correcting vertical land motion from tide gauge records.

From Fig. 3 it is clear that velocity errors have changed sign between these periods in many regional areas (see for instance North America and central/eastern Asia). This change in southeastern Asia, Australia, southern Africa and northern South America may be related with precipitation anomalies during 2010–2011 due to a strong La Niña effect (Boening *et al.* 2012). Large-scale changes in the Southern Ocean and Antarctica may be related with the Antarctic Circumpolar Wave, which has been observed in long-period variations of sea-surface height, temperature, pressure and wind (e.g. Nuncio *et al.* 2011).

4 DISCUSSION

From the analysis of the power-law content in the deformation time-series (see Fig. S1), we deduce that most of the time correlation occurs on the continental landmasses and is driven by continental water mass variations. This is relevant since while corrections for the atmospheric loading are often applied to geodetic observations (e.g. Tregoning & Watson 2009; Dach *et al.* 2011), this is not the dominant contributor to time correlation in most regions. An exception to this is the large contribution of the atmospheric loading to time-correlated deformation in Antarctica (Fig. S1).

A natural question arising on our results is regarding the quality of the loading models and the representativeness of the modelled surface deformation. Even when using model reanalysis, as used here, errors at the interannual periods may arise due to changes in the assimilated observations and to errors in the models. To assess the robustness of our results, we compared the total mass loading deformation described in Section 2 with predictions from the U.S. National Center for Environmental Prediction (NCEP) for the atmospheric contribution (0.25° spatial resolution) and the global ocean reanalyses and simulations (GLORYS; Bernard *et al.* 2006) for the oceanic contribution (0.25°). For the continental water mass contribution, two different models were used, the global

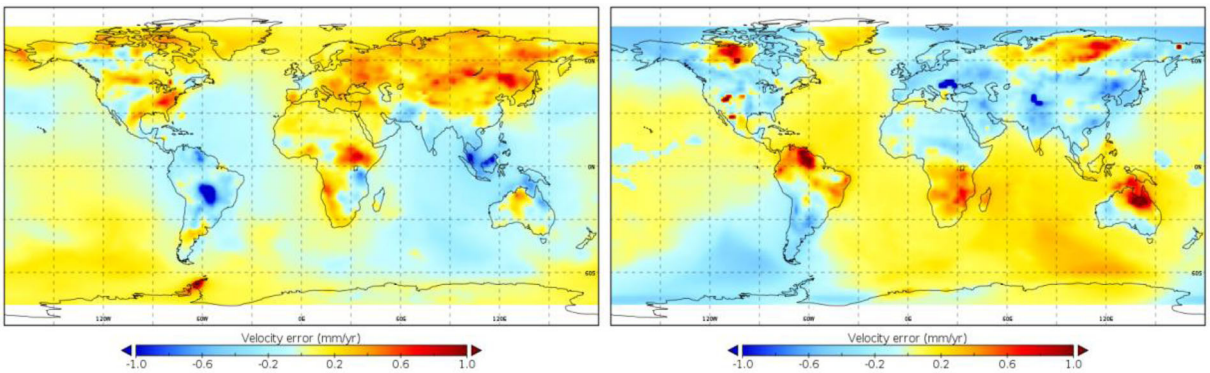

Figure 3. Geographic distribution of the vertical velocity errors (in mm yr^{-1}) for the period 2004–2009 (left-hand panel) and 2009–2014 (right-hand panel) estimated from the total mass loading series with respect to the period 1993–2014.

land data assimilation system (GLDAS/Noah; Rodell *et al.* 2004) and the modern-era retrospective analysis for research and applications (MERRA; Lucchesi 2012), with spatial resolution of 1 and $0.5^\circ \times 0.67^\circ$, respectively. NCEP and GLDAS/Noah deformation predictions were obtained from the Global Geophysical Fluid Center (http://geophy.uni.lu, last accessed May 2015). GLORYS and MERRA deformation predictions were obtained from the University of Strasbourg loading service (http://loading.u-strasbg.fr).

Differences in interannual deformation between the loading models are significant. The modelled deformation used here provides the smallest time correlation while the largest is provided by the combination of NCEP, GLORYS and GLDAS models. Further details on the model comparison are provided in the supporting information. By choosing the models described in Section 2 for our analysis, we present a conservative view of the impact of interannual mass loading on surface velocities with respect to the other models. Moreover, studies have shown higher correlation between ERA Interim and *in situ* observations of precipitation, runoff or gravity than other models (Wang & Zeng 2012; Huang *et al.* 2013; e.g. de Leeuw *et al.* 2014; Mémin *et al.* 2014).

Regarding the representativeness, the modelled deformation does not consider present-day ice mass loss, ground water/aquifers or an Earth response other than elastic. At the interannual period, glacier mass loss is temporally correlated and, additionally, the visco-elastic response of the Earth may have an impact on the surface deformation in places with low viscosity (e.g. Nield *et al.* 2014). Also, the continental water mass models in Greenland and Antarctica are known to be incomplete. In such areas, the actual deformation may be underestimated and our results may be unreliable.

The velocity errors and their spatial pattern shown in Fig. 1 are relevant for geophysical applications using estimated geodetic surface velocities including the determination of coastal sea-level change (e.g. Wöppelmann *et al.* 2014), calibration/validation of satellite altimeters (e.g. Watson *et al.* 2011), tectonic plate motion and deformation (e.g. Tregoning *et al.* 2013), and rheology of the solid Earth including validation/calibration of glacial isostatic adjustment models (King *et al.* 2012b; Mémin *et al.* 2014). Over the two decades analysed, the number of GPS stations has grown continuously, however very few stations have operated over this full period. Among 2667 GPS stations compiled by the International Association of Geodesy Working Group for the densification of the International Terrestrial Reference Frame (ITRF), the time-series length ranges between 3.5 and 16.3 yr (95 per cent) with a median value of 7 yr. Only about 25 per cent of the stations have more than a decade of data. Note that only stations with at least 3 yr of data up to 2013 were considered for the densification (J. Legrand, personal communication, 2014). These results are even more significant if one considers position offsets which populate the GPS position time-series. Position offsets tend to reduce the effective time-series length used to estimate the velocity (Williams 2003b). For instance, the longest segment of continuous observations (between position offsets) per station for the 2667 stations mentioned above is between 2.1 and 12.5 yr (95 per cent), with a median value of 5.5 yr. This value motivated our 5-yr-long analysis in Section 3. Only about 14 per cent of the stations have more than a decade of continuous observations.

5 CONCLUSIONS

We analysed predicted vertical loading deformation induced by changes in atmospheric, oceanic and continental water mass at interannual periods. We found that for most of the Earth surface (discretely sampled by a global grid spaced 2° between $\pm 80^\circ$N/S latitude) the interannual deformation cannot be considered white or time-uncorrelated, but is better characterized by a power-law process.

Considering 5 yr of data, the estimated power-law parameters translated into vertical velocity errors of 0.3 and 0.7 mm yr^{-1}, respectively for the median and 95 per cent of the sampled locations. Over the continental landmasses, these figures reached 0.5 and 1 mm yr^{-1}, respectively, with some regions near the southern Tropic where the velocity errors exceeded 1 mm yr^{-1}. These velocity errors are substantial if one considers, for instance, the range of rates of sea-level rise during the last century, between 1 and 2 mm yr^{-1}. Comparing these errors to GPS vertical velocity uncertainties, at least 4 yr of continuous data are needed in most of the sampled locations to mitigate the effects of the interannual deformation on secular velocities. This figure increases to 10 yr for areas near the southern Tropic.

These velocity errors are conservative in light of the comparison with different models of surface mass loading deformation and also considering possible mass changes not included in the models, for example, present-day ice mass changes. While different models of atmospheric loading are in close agreement, models of ocean loading, and especially continental water, are not. Since continental water mass changes dominate the time-correlated loading deformation in most of the continental landmasses, unless the loading models are improved, there is presently no robust solution to mitigate these errors other than to increase the time-series lengths. When short time-series are used, the velocity error budget should include the effect of the interannual surface loading deformation. This can be approximated by assessing the predicted velocity change between the actual observations and the full period covered by the loading models on a site-by-site basis.

ACKNOWLEDGEMENTS

ASG is a recipient of a FP7 Marie Curie International Outgoing Fellowship (project number 330103). AM was supported by an Australian Research Council Super Science Fellowship (FS110200045). The authors thank Jean-Paul Boy, Tonie Van Dam and Juliette Legrand for making available the loading deformation models and GPS data. Constructive comments by Matt King, Guy Wöppelmann and Christopher Watson helped to improve the manuscript.

REFERENCES

Bernard, B. *et al.*, 2006. Impact of partial steps and momentum advection schemes in a global ocean circulation model at eddy-permitting resolution, *Ocean Dyn.,* **56,** 543–567.

Blewitt, G. & Lavallée, D., 2002. Effect of annual signals on geodetic velocity, *J. geophys. Res.: Solid Earth,* **107,** ETG 9-1–ETG 9-11.

Boening, C., Willis, J.K., Landerer, F.W., Nerem, R.S. & Fasullo, J., 2012. The 2011 La Niña: so strong, the oceans fell, *Geophys. Res. Lett.,* **39,** L19602, doi:10.1029/2012GL053055.

Bos, M.S., Bastos, L. & Fernandes, R.M.S., 2010. The influence of seasonal signals on the estimation of the tectonic motion in short continuous GPS time-series, *J. Geodyn.,* **49,** 205–209.

Dach, R., Böhm, J., Lutz, S., Steigenberger, P. & Beutler, G., 2011. Evaluation of the impact of atmospheric pressure loading modeling on GNSS data analysis, *J. Geod.,* **85,** 75–91.

Dee, D.P. *et al.*, 2011. The ERA-Interim reanalysis: configuration and performance of the data assimilation system, *Quart. J. R. Meteorol. Soc.,* **137,** 553–597.

de Leeuw, J., Methven, J. & Blackburn, M., 2014. Evaluation of ERA-Interim reanalysis precipitation products using England and Wales observations, *Quart. J. R. Meteorol. Soc.,* **141**(688), 798–806.

Dziewonski, A.M. & Anderson, D.L., 1981. Preliminary reference Earth model, *Phys. Earth planet. Inter.,* **25,** 297–356.
Fritsche, M., Döll, P. & Dietrich, R., 2012. Global-scale validation of model-based load deformation of the Earth's crust from continental water mass and atmospheric pressure variations using GPS, *J. Geodyn.,* **59–60,** 133–142.
Groh, A., Ewert, H., Fritsche, M., Rülke, A., Rosenau, R., Scheinert, M. & Dietrich, R., 2014. Assessing the current evolution of the Greenland Ice Sheet by means of satellite and ground-based observations, *Surveys in Geophys*., **35,** 1459–1480.
Huang, Y., Salama, M.S., Krol, M.S., van der Velde, R., Hoekstra, A.Y., Zhou, Y. & Su, Z., 2013. Analysis of long-term terrestrial water storage variations in the Yangtze River basin, *Hydrol. Earth Syst. Sci.,* **17,** 1985–2000.
King, M.A., Bingham, R.J., Moore, P., Whitehouse, P.L., Bentley, M.J. & Milne, G.A., 2012a. Lower satellite-gravimetry estimates of Antarctic sea-level contribution, *Nature,* **491,** 586–589.
King, M.A., Keshin, M., Whitehouse, P.L., Thomas, I.D., Milne, G. & Riva, R.E.M., 2012b. Regional biases in absolute sea-level estimates from tide gauge data due to residual unmodeled vertical land movement, *Geophys. Res. Lett.,* **39,** L14604, doi:10.1029/2012GL052348.
Lucchesi, R., 2012. File Specification for MERRA Products, pp. 82GMAO Office Note No. 1 (Version 2.3).
Mémin, A., Spada, G., Boy, J.-P., Rogister, Y. & Hinderer, J., 2014. Decadal geodetic variations in Ny-Ålesund (Svalbard): role of past and present ice-mass changes, *Geophys. J. Int.,* **198,** 285–297.
Nahmani, S. *et al.*, 2012. Hydrological deformation induced by the West African Monsoon: comparison of GPS, GRACE and loading models, *J. geophys. Res.: Solid Earth,* **117,** B05409, doi:10.1029/2011JB009102.
Nield, G.A. *et al.*, 2014. Rapid bedrock uplift in the Antarctic Peninsula explained by viscoelastic response to recent ice unloading, *Earth planet. Sci. Lett.,* **397,** 32–41.
Nuncio, M., Luis, A.J. & Yuan, X., 2011. Topographic meandering of Antarctic Circumpolar Current and Antarctic Circumpolar Wave in the ice-ocean-atmosphere system, *Geophys. Res. Lett.,* **38,** L13708, doi:10.1029/2011GL046898.
Petrov, L. & Boy, J.-P., 2004. Study of the atmospheric pressure loading signal in very long baseline interferometry observations, *J. geophys. Res.: Solid Earth,* **109,** B03405, doi:10.1029/2003JB002500.
Rodell, M. *et al.*, 2004. The global land data assimilation system, *Bull. Am. Meteorol. Soc.,* **85,** 381–394.
Santamaría-Gómez, A., Bouin, M.-N., Collilieux, X. & Wöppelmann, G., 2011. Correlated errors in GPS position time series: Implications for velocity estimates, *J. geophys. Res.-Solid Earth,* **116,** doi:10.1029/2010JB007701.
Santamaría-Gómez, A., Gravelle, M., Collilieux, X., Guichard, M., Martín Míguez, B., Tiphaneau, P. & Wöppelmann, G., 2012. Mitigating the effects of vertical land motion in tide gauge records using a state-of-the-art GPS velocity field, *Global planet. Change,* **98–99,** 6–17.
Stammer, D., Wunsch, C., Fukumori, I. & Marshall, J., 2002. State estimation improves prospects for ocean research, *EOS, Trans. Am. geophys. Un.,* **83,** 289–295.
Tregoning, P. & Watson, C., 2009. Atmospheric effects and spurious signals in GPS analyses, *J. geophys. Res.: Solid Earth,* **114,** B09403, doi:10.1029/2009JB006344.
Tregoning, P., Burgette, R., McClusky, S.C., Lejeune, S., Watson, C.S. & McQueen, H., 2013. A decade of horizontal deformation from great earthquakes, *J. geophys. Res.: Solid Earth,* **118,** 2371–2381.
Valty, P., de Viron, O., Panet, I., Van Camp, M. & Legrand, J., 2013. Assessing the precision in loading estimates by geodetic techniques in Southern Europe, *Geophys. J. Int.,* **194,** 1441–1454.
van Dam, T., Collilieux, X., Wuite, J., Altamimi, Z. & Ray, J., 2012. Nontidal ocean loading: amplitudes and potential effects in GPS height time series, *J. Geod.,* **86,** 1043–1057.
Van Dam, T.M. & Wahr, J.M., 1987. Displacements of the Earth's surface due to atmospheric loading: effects on gravity and baseline measurements, *J. geophys. Res.: Solid Earth,* **92,** 1281–1286.
Wang, A. & Zeng, X., 2012. Evaluation of multireanalysis products with *in situ* observations over the Tibetan Plateau, *J. geophys. Res.: Atmos.,* **117,** D05102, doi:10.1029/2011JD016553.
Watson, C., White, N., Church, J., Burgette, R., Tregoning, P. & Coleman, R., 2011. Absolute calibration in Bass Strait, Australia: TOPEX, Jason-1 and OSTM/Jason-2, *Mar. Geod.,* **34,** 242–260.
Williams, S.D.P., 2003a. The effect of coloured noise on the uncertainties of rates estimated from geodetic time series, *J. Geod.,* **76,** 483–494.
Williams, S.D.P., 2003b. Offsets in Global Positioning System time series, *J. geophys. Res.: Solid Earth,* **108,** 2310, doi:10.1029/2002JB002156.
Wöppelmann, G. *et al.*, 2013. Is land subsidence increasing the exposure to sea level rise in Alexandria, Egypt?, *Geophys. Res. Lett.,* **40,** 2953–2957.
Wöppelmann, G., Marcos, M., Santamaría-Gómez, A., Martín-Míguez, B., Bouin, M.N. & Gravelle, M., 2014. Evidence for a differential sea level rise between hemispheres over the twentieth century, *Geophys. Res. Lett.,* **41,** 1639–1643.

SUPPORTING INFORMATION

Additional Supporting Information may be found in the online version of this paper:

Figure S1. Geographical distribution of the increment of log-likelihood of power-law noise with respect to white noise (top panel), the power-law spectral index (middle panel) and power-law amplitude (bottom panel) estimated for the vertical non-linear deformation associated with surface mass changes in the atmosphere, oceans, continental hydrology and total mass. The red line in top figures indicates the 2.3 log-likelihood threshold to detect power-law content.

Figure S2. Geographical distribution of the increment of log-likelihood of power-law noise with respect to white noise (top left-hand panel), the power-law spectral index (top right-hand panel), the power-law amplitude (bottom left-hand panel), and the velocity errors for 5 yr of continuous data using monthly sampling (bottom right-hand panel). These quantities were estimated from the horizontal non-linear deformation associated with the total surface mass changes (atmosphere, oceans and continental hydrology). The red line in top left-hand figure indicates the 2.3 log-likelihood threshold to detect power-law content.

Figure S3. Geographic distribution of the vertical velocity errors (in mm yr^{-1}) for 5 yr of continuous data. Velocity errors are computed from the 2σ standard deviation of trends estimated from the total deformation time-series in 5-yr-long overlapping periods between 1993 and 2014.

Figure S4. Geographic distribution of the 150 sites used to compare the deformation loading models. Open circles represent sites were power-law was not found in the total deformation time-series.

Figure S5. Comparison of vertical velocity uncertainty (in mm yr^{-1}) for 5-yr-long time-series transformed from power-law noise estimates between ERA Interim and NCEP (left-hand panel), ECCO and GLORYS (middle panel) and ERAint + ECCO + ERAint (right-hand panel, horizontal axis) and NCEP + GLORYS + MERRA (right-hand panel, red dots, vertical axis) and NCEP + GLORYS + GLDAS (right-hand panel, blue dots, vertical axis). Note the scale change in the rightmost plot.
(http://gji.oxfordjournals.org/lookup/suppl/doi:10.1093/gji/ggv190/-/DC1)

Please note: Oxford University Press is not responsible for the content or functionality of any supporting materials supplied by the authors. Any queries (other than missing material) should be directed to the corresponding author for the paper.